The Astrophysical Journal Letters, 933:L13 (7pp), 2022 July 1 https://doi.org/10.3847/2041-8213/ac786d
© 2022. The Author(s). Published by the American Astronomical Society.
OPEN ACCESS

60 Candidate High-velocity Stars Originating from the Sagittarius Dwarf Spheroidal Galaxy in Gaia EDR3

Hefan Li[1], Cuihua Du[2], Jun Ma[2,3], Jianrong Shi[2,3], Heidi Jo Newberg[4], and Yunsong Piao[1]
[1] School of Physical Sciences, University of Chinese Academy of Sciences, Beijing 100049, People's Republic of China; ducuihua@ucas.ac.cn
[2] College of Astronomy and Space Sciences, University of Chinese Academy of Sciences, Beijing 100049, People's Republic of China
[3] Key Laboratory of Optical Astronomy, National Astronomical Observatories, Chinese Academy of Sciences, Beijing 100012, People's Republic of China
[4] Department of Physics, Applied Physics and Astronomy, Rensselaer Polytechnic Institute, Troy, NY 12180, USA
Received 2022 January 5; revised 2022 June 8; accepted 2022 June 14; published 2022 June 30

Abstract

Using proper motions from Gaia Early Data Release 3 (Gaia EDR3) and radial velocities from several surveys, we identify 60 candidate high-velocity stars with a total velocity greater than 75% of the escape velocity that probably originated from the Sagittarius dwarf spheroidal galaxy (Sgr) by orbital analysis. Sgr's gravity has little effect on the results and the Large Magellanic Cloud's gravity has a nonnegligible effect on only a few stars. The closest approach of these stars to the Sgr occurred when the Sgr passed its pericenter (∼38.2 Myr ago), which suggests they were tidally stripped from the Sgr. The positions of these stars in the Hertzsprung–Russell diagram and the chemical properties of 19 of them with available [Fe/H] are similar to the Sgr stream member stars. This is consistent with the assumption of their accretion origin. Two of the 60 are hypervelocity stars, which may also be produced by the Hills mechanism.

Unified Astronomy Thesaurus concepts: High-velocity stars (736); Stellar dynamics (1596); Sagittarius dwarf spheroidal galaxy (1423); Stellar abundances (1577); Hertzsprung Russell diagram (725)

1. Introduction

High-velocity stars move so fast that they imply the presence of extreme dynamical processes. One type of high-velocity star is a hypervelocity star (HVS), which has an extreme velocity above the escape velocity of the Milky Way. Hills (1988) first theoretically predicted the formation of HVSs by a close encounter between a binary system and the massive black hole (MBH) in the Galactic Center (GC). Yu & Tremaine (2003) analyze the ejection mechanism of single stars and a binary MBH and calculate the ejection rate. The first candidate HVS was discovered by Brown et al. (2005), a B-type star with a total velocity of 709 km s^{-1} in the Galactic halo. Recently, the Southern Stellar Stream Spectroscopic Survey (S^5) discovered the currently fastest HVS known (Koposov et al. 2020): An A-type star with a total velocity of 1755 km s^{-1} located at a heliocentric distance of ∼9 kpc whose backward orbit was found to point unambiguously to the GC, providing direct evidence of the Hills mechanism.

Runaway stars are another type of high-velocity star; their velocity often points away from an OB association. One mechanism to produce a runaway star is to be ejected in binaries when its companion has exploded as a supernova (Blaauw 1961; Tauris & Takens 1998; Portegies Zwart 2000; Wang & Han 2009; Wang et al. 2013). Tauris (2015) investigated the ejection velocity of early- and late-type stars under this mechanism, and they found that the upper limit of the ejection velocity of B stars (∼10$M_\odot$) can reach 550 km s^{-1} in the Galactic rest frame and that late-type stars are even faster. The other mechanism is ejection from a stellar system by dynamical interactions (Poveda et al. 1967). Gvaramadze et al. (2009) explored the exchange encounters in a three-body system and found that the ejected star can obtain velocities of ∼200–400 km s^{-1}, depending on its mass. The discoveries of HVS US 708 (Geier et al. 2015) and HD 271791 (Heber et al. 2008) provide strong support for the two mechanisms.

Besides the mechanisms mentioned above, high-velocity stars could also be ejected by other mechanisms such as from the tidal debris of disrupted dwarf galaxies or the gravitational slingshot effect (e.g., Boubert & Evans 2016; García-Bellido 2017; Montanari et al. 2019). Abadi et al. (2009) used simulations to predict that HVS can be ejected from tidally disrupted dwarf galaxies. A close interaction between a globular cluster and a single supermassive black hole or a binary supermassive black hole could lead to the ejection of high-velocity stars (Capuzzo-Dolcetta & Fragione 2015; Fragione & Capuzzo-Dolcetta 2016). The HVS HE 0437-5439 is suggested to be ejected from the Large Magellanic Cloud (LMC) through the Hills mechanism (Erkal et al. 2019a). Du et al. (2018, 2019) use Gaia and LAMOST data to discover that some high-velocity stars originate from the tidal debris of disrupted dwarf galaxies. Caffau et al. (2020) used Gaia DR2 and VLT data to present the chemodynamical investigation of 72 high-velocity sample stars and suggested that these stars can be the result of a disrupted small galaxy or globular cluster members. Marchetti (2021) derived that seven high-velocity stars possibly originate from an extragalactic origin from Gaia EDR3. All of these results provide strong evidence that high-velocity stars originate from accreted and disrupted dwarf spheroidal galaxies. However, most studies could not judge which dwarf galaxy or globular cluster these high-velocity stars originate from. Recently, Huang et al. (2021) discovered a candidate HVS (J1443+1453) with a total velocity of 559 km s^{-1} that is probably from the Sagittarius dwarf spheroidal galaxy (Sgr).

In this Letter, we report the discovery of 60 candidate high-velocity stars that probably originated from the Sgr. Among them are two HVS candidates with extreme velocity that could

Original content from this work may be used under the terms of the Creative Commons Attribution 4.0 licence. Any further distribution of this work must maintain attribution to the author(s) and the title of the work, journal citation and DOI.

have been produced by the Hills mechanism, requiring a central MBH in the Sgr. This Letter is organized as follows: In Section 2, we describe the method of assembling sample high-velocity stars. Section 3 explores the possible origin of sample stars by orbital analysis. Finally, we give a summary and discussion in Section 4.

2. Samples

Gaia Early Data Release 3 (Gaia EDR3; Collaboration et al. 2021) provides positions, proper motions, and parallaxes for about 1.468 billion sources. It also contains radial velocities (*rv*'s) for about 7.21 million stars from Gaia DR2 (Collaboration et al. 2018). Furthermore, we cross-match the Gaia EDR3 catalog with the Gaia-ESO DR4 (Gilmore et al. 2012; Randich et al. 2013), the Galactic Archaeology with HERMES (GALAH) DR3 (De Silva et al. 2015; Buder et al. 2021), low- and medium-resolution spectra (LRS and MRS) of the Large Sky Area Multi-object Fiber Spectroscopic Telescope (LAMOST) DR9 (Cui et al. 2012; Zhao et al. 2012; Liu et al. 2020), the Radial Velocity Experiment (RAVE) DR6 (Steinmetz et al. 2020a, 2020b), the Sloan Digital Sky Surveys (SDSS) optical spectra DR17 (York et al. 2000; Yanny et al. 2009; Abdurro'uf et al. 2022), the Apache Point Observatory Galactic Evolution Experiment (APOGEE, Majewski et al. 2017) of SDSS DR17, and the Southern Stellar Stream Spectroscopic Survey (S^5) DR1 (Li et al. 2019) to supplement the *rv*) information.

We select stars with RUWE < 1.4, where RUWE (renormalized unit weight error) is a reliable and informative goodness-of-fit statistic in Gaia EDR3 (Lindegren et al. 2021b). We use the Lindegren et al. (2021a) method to correct the Gaia EDR3 parallaxes (ϖ) and remove stars $\varpi < 5\sigma_{\varpi}$. For spectroscopic data, we require $\mathrm{S/N} > 10$.

We use the median value of the *rv* difference $\delta v = rv_{\mathrm{survey}} - rv_{\mathrm{Gaia}}$ to correct the *rv* offset of other surveys relative to Gaia, and the results are listed in Table 1.

The misestimation of the *rv* error is reported in many studies (e.g., Cottaar et al. 2014; Tsantaki et al. 2022). Following the method outlined in Li et al. (2019), we use the mixture model

$$\delta v_{i,j} \sim f\mathcal{N}(0, \sqrt{F^2(\sigma_{v,i}) + F^2(\sigma_{v,j})}) + (1-f)\mathcal{N}(0, \sigma_{\mathrm{outl}}), \tag{1}$$

where $\delta v_{i,j}$ is the pairwise *rv* difference, f is the weight of the first mixture component, $\sigma_{v,i}$ and $\sigma_{v,j}$ are the *rv* errors of the ith and jth observations, respectively, and σ_{outl} is the outlier of the *rv* difference. The *rv* correction function is $F(\sigma_v) = \sqrt{(k \times \sigma_v)^2 + \sigma_{v,\mathrm{floor}}^2}$, where k is the correction factor and $\sigma_{v,\mathrm{floor}}$ is the floor error of the *rv*.

For surveys with at least 10^4 sources that contain multiple observations, we fit this model to multiple observations. The results are listed in Table 1 and the correction method of these surveys in Table 1 is set to "dupl." In addition, the *rv* error in the S^5 catalog has been corrected based on this method (Li et al. 2019).

We apply a similar method to other surveys. In Equation (1), the ith observation is from only one of the uncorrected surveys, and the jth observation is from all corrected surveys. The results are also listed in Table 1 and the method is marked as "cross."

Table 1
Correction Parameters for the Radial Velocity and Its Error

Survey	offset km s^{-1}	k	$\sigma_{v,\mathrm{floor}}$ km s^{-1}	Method
LAMOST LRS	−5.11	0.81	0.0	dupl
LAMOST MRS	−0.82	0.99	1.78	dupl
APOGEE	−0.09	1.78	0.08	dupl
RAVE	−0.32	0.92	0.89	dupl
SDSS	7.69	1.41	2.2	dupl
S^5	−0.35	⋯	⋯	⋯
GALAH	−0.32	2.92	0.31	cross
Gaia-ESO	−0.3	3.33	0.0	cross
Gaia	⋯	1.56	0.3	cross

Note. Column 1 is the survey name. Column 2 lists the *rv* offset from Gaia. Columns 3–4 are the correction parameters applied in Equation (1). Column 5 gives the correction method used.

After applying the above corrections, we weight the *rv* means by the inverse of its variance. Observations that deviate from the average by more than 3σ are removed. We only retain stars with the epoch number of *rv*, $n_{rv} \geqslant 4$ to ensure that the *rv* can be considered as the systemic velocity of the system (Boubert et al. 2019).

To search for stars that originated from dwarf galaxies or globular clusters in our sample, we collect 50 dwarf galaxies and 160 globular clusters. Forty-six dwarf galaxies are referenced from Li et al. (2021). We add Leo T, Pegasus III, Phoenix I (McConnachie & Venn 2020a), and Sgr (Fritz et al. 2018) to our dwarf galaxy sample. All 160 globular clusters are referenced from Vasiliev & Baumgardt (2021).

Heliocentric distances (d) and velocities in the R.A. and decl. direction (v_α and v_δ) are derived using the Bayesian method (Luri et al. 2018). We use the posterior of Du et al. (2019) and replace the distance prior with the three-parameter Generalized Gamma Distribution (Bailer-Jones et al. 2021). The priors for both v_α and v_δ are uniform. We use the Markov Chain Monte Carlo (MCMC) sampler, emcee (Foreman-Mackey et al. 2013), to draw samples from the posterior probability. The distances and velocities of dwarf galaxies and globular clusters are calculated using a similar method. Due to the high accuracy of their distance modulus and distance, we use uniform distributions as distance priors. In this study, we generate 2000 Monte Carlo (MC) realizations for each object (stars, dwarf galaxies, and globular clusters) and use the median value to describe the results. The lower and upper uncertainties are the 16th and 84th percentiles of the probability distribution function.

We use the right-handed Cartesian Galactocentric coordinate system (Jurić et al. 2008). Here we adopt the distance of the Sun to the GC, $R_\odot = 8.122$ kpc (Gravity Collaboration et al. 2018) and the vertical distance from the Sun to the Galactic midplane $z_\odot = 25$ pc (Jurić et al. 2008). The proper motions, *rv*'s, and distances are used to derive 3D velocities (U, V, W) in the right-handed coordinate system (Johnson & Soderblom 1987).

To get an accurate high-velocity star sample, we select stars with $\sigma_{v_{\mathrm{GC}}}/v_{\mathrm{GC}} < 30\%$ and $v_{\mathrm{GC}} > 0.75 v_{\mathrm{esc}}(\boldsymbol{r})$, where v_{GC} and σv_{GC} are the Galactic total velocity and its error, and $v_{\mathrm{esc}}(\boldsymbol{r})$ is the escape velocity at $\boldsymbol{r} = (x, y, z)$ in the Eilers et al. (2019) potential model, which includes a Plummer (Binney & Tremaine 1987) bulge, two Miyamoto-Nagai (Miyamoto & Nagai 1975) disks, and an NFW (Navarro–Frenk–White;

Navarro et al. 1997) dark matter halo. By applying the above selection criteria, we obtain 1049 sample stars.

3. Orbit Analysis

To get some hints on the ejection location of our sample high-velocity stars, we study their orbit by adopting the potential model in Eilers et al. (2019) We use `galpy` (Bovy 2015) to get the orbit of our Bayesian samples (stars, dwarf galaxies, and globular clusters), and integrate the orbit back over a total time of 1 Gyr. The gravitational influence of the dwarf galaxy and globular cluster is temporarily ignored.

We define the normalized distance from the star to the dwarf galaxy and to the globular cluster:

$$\Delta r^*_{\rm affi} = \begin{cases} \frac{|\boldsymbol{r}_{\rm star} - \boldsymbol{r}_{\rm dwarf}|}{r_{\rm half}}, & \text{for dwarf galaxies} \\ \frac{|\boldsymbol{r}_{\rm star} - \boldsymbol{r}_{\rm cluster}|}{R_0}, & \text{for globular clusters,} \end{cases} \quad (2)$$

where $\boldsymbol{r} = (x,\ y,\ z)$ is Galactocentric coordinates, d is the heliocentric distance, $r_{\rm half}$ is the half-light radius, and R_0 is the scale radius of the Plummer model (Vasiliev & Baumgardt 2021). Most of the $r_{\rm half}$ are referenced from McConnachie & Venn (2020b) except Crater I (Laevens et al. 2014). The relative minimum value of $\Delta r^*_{\rm affi}$ is marked as $\Delta r^*_{\rm min}$. If there are multiple relative minima, we take the nth one that maximizes the probability that the star originated from the dwarf galaxy or the globular cluster $P_{\rm affi}$. This probability is defined as the fraction of MC realizations with $\Delta r^*_{\rm min} < 2.5$.

There are 60 stars with $P_{\rm Sgr} > 50\%$, which means the probability of these stars originating from the Sgr is greater than 50%. We have not found any stars with a probability of originating from other dwarf galaxies or globular clusters greater than 50%. The maximum probability of originating from non-Sgr objects is 11.4%, and this possible object is Antlia II with a half-light radius of 2.95 kpc. The maximum probability that a star originates from globular clusters is 6.3%, and the possible source is ω Cen with a scale radius of 23 pc. To test the influence of Sgr's large half-light radius, we create a "mirror" Sgr by reversing the sign of Sgr's z and v_z. Based on the same method as above, we find 24 stars with $P_{\rm mirror} > 50\%$, which is less than half of the number of stars originating from Sgr.

In order to further determine the link between these stars and Sgr, we use `GIZMO` (Springel 2005; Hopkins 2015) to take the gravitational influence of Sgr into account by assuming a Keplerian potential with a total mass of $4 \times 10^8 M_\odot$ for Sgr (Vasiliev & Belokurov 2020). We select 215 stars with $\Delta r^*_{\rm min} < 5.5$ relative to the Sgr and repeat the above orbit analysis in a total time of 0.5 Gyr. The change in $\Delta r^*_{\rm min}$ is very small, equivalent to several parsecs. This is approximately equal to the half-light radius of most globular clusters; therefore, the globular cluster $\Delta r^*_{\rm min}$ is very sensitive to the gravitational potential. The probability of stars originating from a globular cluster is therefore greatly affected. But dwarf galaxies ($r_{\rm half} \sim 100$ pc) are hardly affected.

The Large Magellanic Cloud (LMC) with a mass of $1.38 \times 10^{11} M_\odot$ (Erkal et al. 2019b) is an important gravitational source in the Milky Way. Its proper motions are referenced from Gaia Collaboration et al. (2021), and other parameters are from McConnachie & Venn (2020a). We also use the Bayesian method to obtain 2000 random samples. Because of its distance, it is considered a point source. For most of our selection of 215 stars, the change in $\Delta r^*_{\rm min}$ is less than 100 pc compared to only considering the Sgr's gravity. The $\Delta r^*_{\rm min}$ of dwarf galaxies with a smaller half-light radius may be significantly affected. The change in $\Delta r^*_{\rm min}$ for eight stars is more than 1 kpc, and the maximum value is 7.9 kpc.

Finally, there are 60 stars with $P_{\rm Sgr} > 50\%$. The distribution of these stars in $v_{\rm GC}$ and $r_{\rm GC}$ space is shown in Figure 1. We also plot the escape velocity curve of four Milky Way potential models (Bovy 2015; McMillan 2017; Eilers et al. 2019; Cautun et al. 2020) as a function of Galactocentric distance in this figure.

Figure 2 shows the properties of stars at the time of the closest approach. In panel (a), we show the distribution of the velocity difference versus the half-light radius normalized distance between the star and the Sgr when they are the closest approach. We consider the velocity of the stars relative to Sgr as their ejection velocity $v_{\rm ej}$. There are 2 stars with $v_{\rm ej} \sim 740\ {\rm km\,s^{-1}}$, such a fast velocity may be produced by the Hills mechanism (Hills 1988; Bromley et al. 2006). The probability of an ejection is

$$P_{\rm ej} \approx \begin{cases} 1 - D_{\rm min}/175, & \text{if } 0 \leqslant D_{\rm min} \leqslant 175 \\ 0, & \text{otherwise,} \end{cases} \quad (3)$$

where

$$D_{\rm min} = \frac{R_{\rm min}}{a_{\rm bin}} \left[\frac{2M_{\rm bh}}{10^6 (m_1 + m_2)} \right]^{-1/3}, \quad (4)$$

where $R_{\rm min}$ is the distance between the binary and the black hole during the close encounter, $a_{\rm bin}$ is the semimajor axis of the binary, and $M_{\rm bh}$, m_1, and m_2 are the masses of the black hole and the binary, respectively. However, $R_{\rm min}$ (i.e., $\Delta r_{\rm min}$ in our study) is much larger than a reasonable binary semimajor axis for our candidate stars. This indicates $D_{\rm min} > 175$, so $P_{\rm ej} = 0$. This does not mean that the Hills mechanism is not a reasonable explanation for the candidate Sgr HVSs, because the orbital uncertainty could increase $D_{\rm min}$ to more than 175. The small error in $\Delta r_{\rm min}$ suggests that statistical error is not the main reason. Additional gravitational influences may cause changes in the orbits of stars after they are ejected, such as the globular clusters associated with the Sgr (Ibata et al. 1995; NGC 6715 (M54), Terzan 7, Arp 2, and Terzan 8) and Sgr stream. Therefore, the mass of the black hole cannot be estimated, which needs to be further studied with N-body simulations in the future.

Another ejection mechanism for high-velocity stars is the tidal disruption of the dwarf galaxy (Abadi et al. 2009). Their simulation shows that during the last time the dwarf galaxy passed through the pericenter, the velocity distribution of the stars in the tidal debris extended beyond the escape velocity. As shown in panel (b) of Figure 2, the backward time $t_{\rm trace}$ of the closest approach and when the Sgr passed its pericenter are close for 59 stars with $P_{\rm Sgr} > 50\%$ (except one star with $t_{\rm trace} \sim 150$ Myr). This is consistent with the results from Abadi et al. (2009). With the release of more high-precision data, we could discover more high-velocity stars from the accreted and disrupted dwarf spheroidal galaxies, which would help us better understand the property of dwarf galaxies and the history of the Milky Way's accretion.

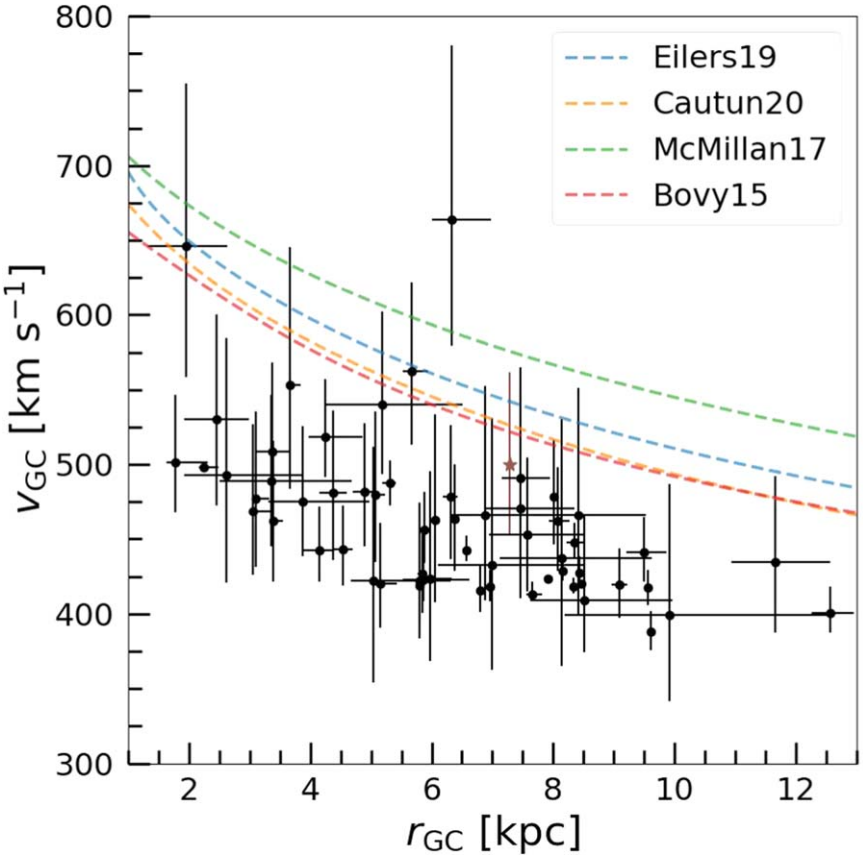

Figure 1. Distribution of total velocity v_{GC} vs. Galactocentric distance r_{GC} for stars with $P_{Sgr} > 50\%$. Black points with error bars represent stars with the probability of correlation with Sgr $P_{Sgr} > 0.5$. The brown star with error bars is the candidate star that is probably from the Sgr found by Huang et al. (2021). The four different colored dashed lines are the escape velocity curves derived from the different Milky Way potential models (Bovy 2015; McMillan 2017; Eilers et al. 2019; Cautun et al. 2020).

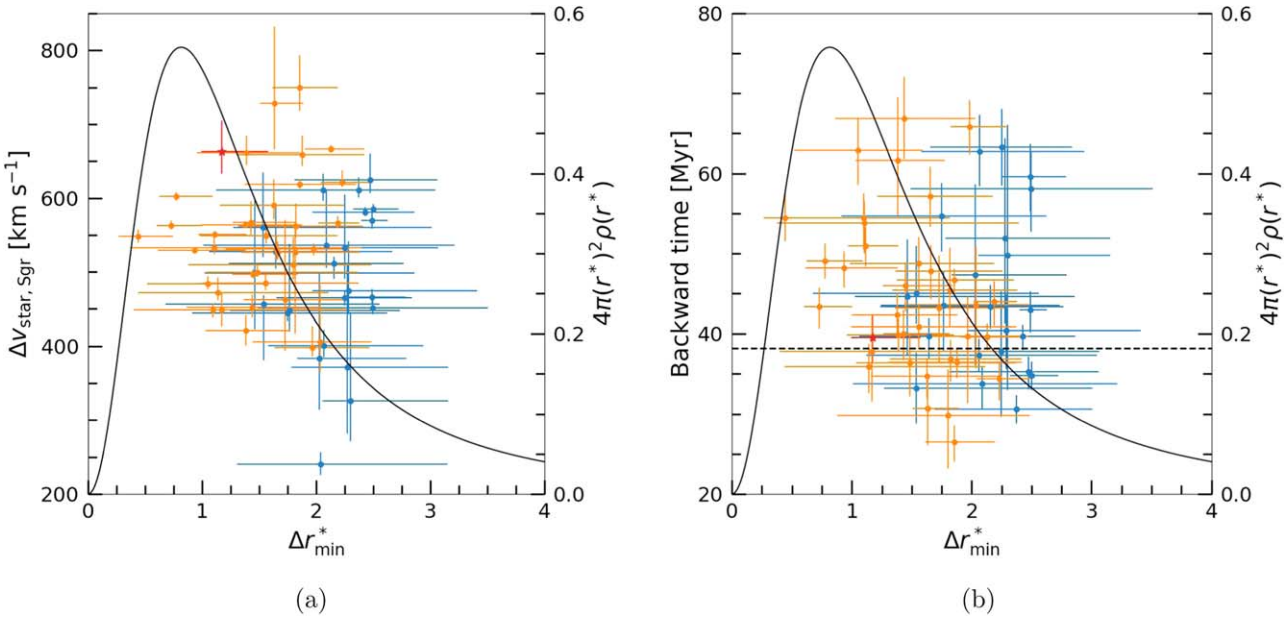

Figure 2. Panel (a): Distribution of the velocity and the half-light radius normalized distance of stars relative to the Sgr when they are at the closest point. Stars with probability $P_{Sgr} > 50\%$ originating from the Sgr are shown in blue points. Orange points represent stars with a probability of $P_{Sgr} > 84\%$. The black line shows the density at the spherical shell as a function of the half-light radius normalized distance from the Sgr center. The candidate star probably from Sgr found by Huang et al. (2021) is shown in the red star. Panel (b): Backward time vs. normalized distance between the star and the Sgr during the closest approach. The symbols are the same as in panel (a). The black horizontal dashed line shows the backward time when the Sgr arrives at its pericenter.

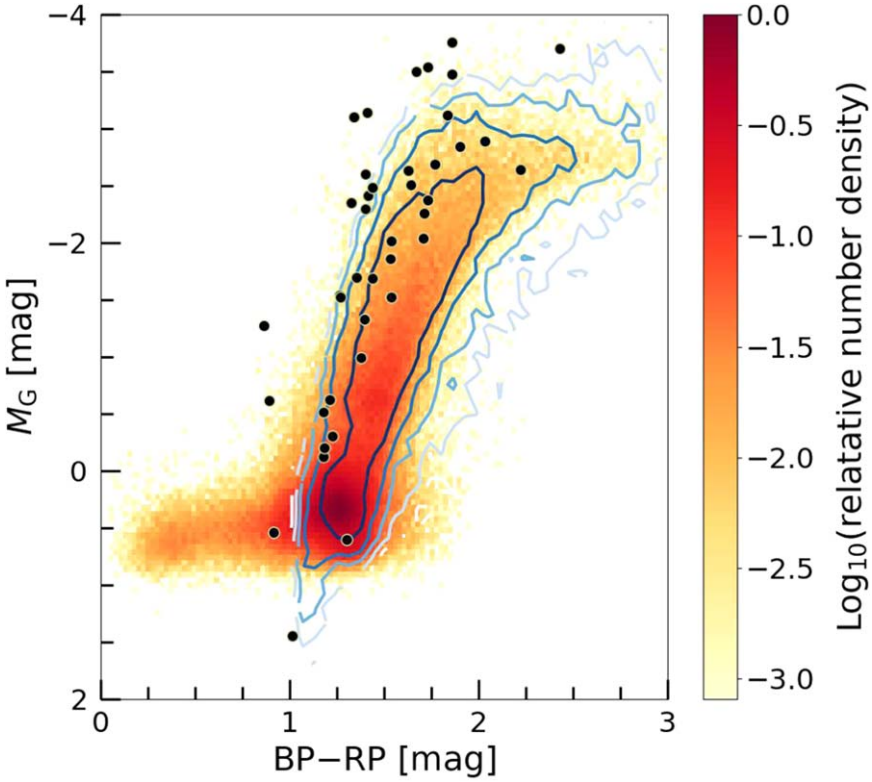

Figure 3. Color–magnitude diagram of stars with probability originating from the Sgr greater than 50% (black points) compared to the Sgr (red pixels; Vasiliev & Belokurov 2020) and the Sgr stream (blue contour lines; Vasiliev et al. 2021). The color of the pixel is coded by the logarithmic number density relative to the maximum density. The contour lines are equal logarithmic number density lines with an interval of 0.5 dex.

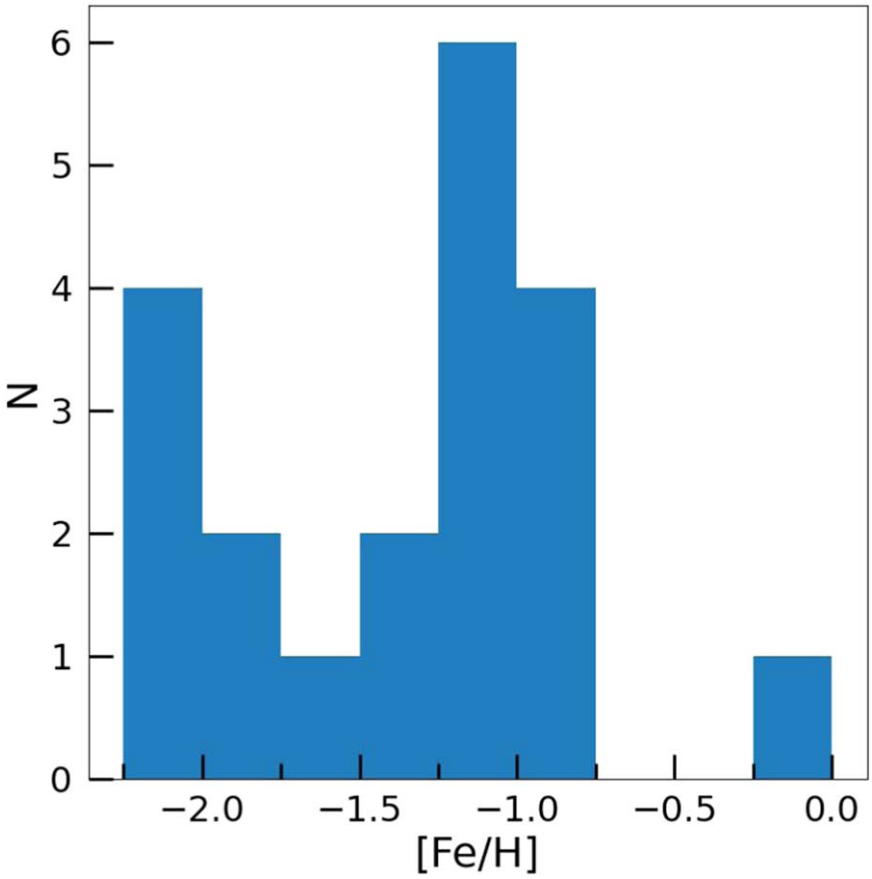

Figure 4. Histogram of the metallicity distribution of stars with probability originating from Sgr greater than 50%.

Figure 3 shows the Hertzsprung–Russell (HR) diagram for stars with the probability $P_{\rm Sgr} > 50\%$. The x-axis is the color index in the Gaia BP band and RP band. The y-axis is the Gaia G-band absolute magnitude, which is corrected by the extinction provided by Green et al. (2019). All of them are late-type giant stars. As shown in this figure, these high-velocity Sgr stars are most similar to both the Sgr and Sgr stream, but they are closer to the Sgr stream relative to the Sgr, which is more concentrated at ($M_{\rm G}$, BP − RP) = (0.5, 1.25). This suggests that these stars have a similar origin to the Sgr stream.

Of the 60 stars with $P_{\rm Sgr} > 50\%$, only 19 have metallicity information, the distribution is shown in Figure 4. There are two peaks in this distribution. The first one is at $[{\rm Fe/H}] \sim -1$, which is very close to the metallicity distribution of the Sgr stream (Hayes et al. 2020). This is consistent with the assumption that they are tidally stripped stars from the Sgr. The peak at $[{\rm Fe/H}] \sim -2$ is close to the metal-poorest part of the Sgr stream, and they may originate from the Sgr halo. One metal-rich star ($[{\rm Fe/H}] = -0.03$) reaches the upper limit of the Sgr's metallicity and has a retrograde orbit. It is located at ($M_{\rm G}$, BP − RP) = (0.6, 1.3) in Figure 3, very close to the densest region of Sgr ($M_{\rm G}$, BP − RP) = (0.5, 1.25) and may be related to the metal-richest part of Sgr.

Recently, Huang et al. (2021) discovered a candidate high-velocity star originating from Sgr. It is not included in our sample because its rv is based only on two epochs. We test this star using our method and find similar results. It is shown in Figure 1 and Figure 2. Our determined minimum distance $\Delta r_{\rm min} = 3.33^{+1.09}_{-0.51}$ kpc, the trace-back time $t_{\rm trace} = 39.4^{+2.6}_{-3.2}$ Myr, and the velocity difference $\Delta v = 665^{+43}_{-30}$ km s^{-1} correspond to their results: $\Delta r_{\rm min} = 2.42^{+1.8}_{-0.77}$ kpc, $t_{\rm trace} = 37.8^{+4.6}_{-6.0}$ Myr, and $\Delta v = 690^{+104}_{-65}$ km s^{-1}. This difference has little effect on dwarf galaxies with a large half-light radius like Sgr, but it may have an effect on some dwarf galaxies with a small half-light radius.

4. Summary and Discussion

In this Letter, based on the high-quality positions, proper motions, and parallaxes of Gaia EDR3 combined with the rv of several surveys, we define a high-velocity star sample with $v_{\rm GC} > 0.75 v_{\rm esc}$. By analyzing backward orbits, we investigate the links between these stars and 50 dwarf galaxies and 160 globular clusters. Finally, there are 60 stars that had a closest approach with Sgr. The encounter time is close to when Sgr reached its pericenter and all of them are late-type giants. A catalog of the properties of these stars is available at https://nadc.china-vo.org/res/r101121/.

The effect of the Sgr's gravity can be ignored. Even further considering the gravity of the LMC, very few stars are significantly affected. The similarity of the 60 stars and the Sgr stream in the HR diagram suggests they could be from the Sgr. Nineteen of these stars with available [Fe/H] are also chemically similar to the Sgr stream. Moreover, we found two HHVSs with an ejection velocity $v_{\rm ej} \sim 740$ km s^{-1}. This extreme velocity can be produced by the Hills mechanism (Hills 1988), but it is difficult to constrain the properties of black holes at the center of the Sgr.

Because Sgr has just passed its pericenter (∼38.2 Myr ago), we could expect to discover more high-velocity stars originating from Sgr with the release of more and more large-survey data. The details, such as the number and velocity distribution, need to be studied using numerical simulations. This can help us study the interaction between the Sgr and the Milky Way in the accretion event, which will provide important clues to the formation and evolution history of the Milky Way galaxy. On the other hand, most of the dwarf galaxies discovered are located near their pericenter (Li et al. 2021). This means that we can better study the high-velocity stars of tidal origin, and it is helpful for understanding the different ejection mechanisms of high-velocity stars.

We thank especially the referee for the insightful comments and suggestions, which have improved the paper significantly. This work was supported by the National Natural Foundation of China (NSFC Nos. 11973042, 11973052, and 11873053). It was also supported by the Fundamental Research Funds for the Central Universities and the National Key R&D Program of China No. 2019YFA0405501. H.J.N. acknowledges funding from US NSF grant AST-1908653. This project was developed in part at the 2016 NYC Gaia Sprint, hosted by the Center for Computational Astrophysics at the Simons Foundation in New York City.

This work has made use of data from the European Space Agency (ESA) mission Gaia (https://www.cosmos.esa.int/gaia), processed by the Gaia Data Processing and Analysis Consortium (DPAC, https://www.cosmos.esa.int/web/gaia/dpac/consortium). Funding for the DPAC has been provided by national institutions, in particular the institutions participating in the Gaia Multilateral Agreement.

This work made use of the Third Data Release of the GALAH Survey. This paper includes data that has been provided by AAO Data Central (datacentral.aao.gov.au). It also made use of the Sixth Data Release of the RAVE Survey. Guoshoujing Telescope (the Large Sky Area Multi-Object Fiber Spectroscopic Telescope LAMOST) is a National Major Scientific Project built by the Chinese Academy of Sciences. Funding for the project has been provided by the National Development and Reform Commission. Funding for the Sloan Digital Sky Survey IV has been provided by the Alfred P. Sloan Foundation, the US Department of Energy Office of Science, and the Participating Institutions. SDSS-IV acknowledges support and resources from the Center for High Performance Computing at the University of Utah. The SDSS website is www.sdss.org. Based on data acquired at the Anglo-Australian Telescope. We acknowledge the traditional owners of the land on which the AAT stands, the Gamilaraay people, and pay our respects to elders past and present.

ORCID iDs

Hefan Li https://orcid.org/0000-0002-9497-8127
Cuihua Du https://orcid.org/0000-0002-3954-617X
Jun Ma https://orcid.org/0000-0001-6329-6644
Jianrong Shi https://orcid.org/0000-0002-0349-7839
Heidi Jo Newberg https://orcid.org/0000-0001-8348-0983

References

Abadi, M. G., Navarro, J. F., & Steinmetz, M. 2009, ApJL, 691, L63
Abdurro'uf, Accetta, A. K., Aerts, C., et al. 2022, ApJS, 259, 35
Bailer-Jones, C. A. L., Rybizki, J., Fouesneau, M., Demleitner, M., & Andrae, R. 2021, AJ, 161, 147
Binney, J., & Tremaine, S. 1987, Galactic dynamics (Princeton, NJ: Princeton Univ. Press), 747
Blaauw, A. 1961, BAN, 15, 265
Boubert, D., & Evans, N. W. 2016, ApJL, 825, L6

Boubert, D., Strader, J., Aguado, D., et al. 2019, MNRAS, 486, 2618
Bovy, J. 2015, ApJS, 216, 29
Bromley, B. C., Kenyon, S. J., Geller, M. J., et al. 2006, ApJ, 653, 1194
Brown, W. R., Geller, M. J., Kenyon, S. J., & Kurtz, M. J. 2005, ApJL, 622, L33
Buder, S., Sharma, S., Kos, J., et al. 2021, MNRAS, 506, 150
Caffau, E., Monaco, L., Bonifacio, P., et al. 2020, A&A, 638, A122
Capuzzo-Dolcetta, R., & Fragione, G. 2015, MNRAS, 454, 2677
Cautun, M., Benítez-Llambay, A., Deason, A. J., et al. 2020, MNRAS, 494, 4291
Collaboration, G., Brown, A. G. A., Vallenari, A., et al. 2018, A&A, 616, A1
Collaboration, G., Brown, A. G. A., Vallenari, A., et al. 2021, A&A, 649, A1
Cottaar, M., Covey, K. R., Meyer, M. R., et al. 2014, ApJ, 794, 125
Cui, X.-Q., Zhao, Y.-H., Chu, Y.-Q., et al. 2012, RAA, 12, 1197
De Silva, G. M., Freeman, K. C., Bland-Hawthorn, J., et al. 2015, MNRAS, 449, 2604
Du, C., Li, H., Newberg, H. J., et al. 2018, ApJL, 869, L31
Du, C., Li, H., Yan, Y., et al. 2019, ApJS, 244, 4
Eilers, A.-C., Hogg, D. W., Rix, H.-W., & Ness, M. K. 2019, ApJ, 871, 120
Erkal, D., Boubert, D., Gualandris, A., Evans, N. W., & Antonini, F. 2019a, MNRAS, 483, 2007
Erkal, D., Belokurov, V., Laporte, C. F. P., et al. 2019b, MNRAS, 487, 2685
Foreman-Mackey, D., Hogg, D. W., Lang, D., & Goodman, J. 2013, PASP, 125, 306
Fragione, G., & Capuzzo-Dolcetta, R. 2016, MNRAS, 458, 2596
Fritz, T. K., Battaglia, G., Pawlowski, M. S., et al. 2018, A&A, 619, A103
Gaia Collaboration, Luri, X., Chemin, L., et al. 2021, A&A, 649, A7
García-Bellido, J. 2017, JPhCS, 840, 012032
Geier, S., Fürst, F., Ziegerer, E., et al. 2015, Sci, 347, 1126
Gilmore, G., Randich, S., Asplund, M., et al. 2012, Msngr, 147, 25
Gravity Collaboration, Abuter, R., Amorim, A., et al. 2018, A&A, 615, L15
Green, G. M., Schlafly, E., Zucker, C., Speagle, J. S., & Finkbeiner, D. 2019, ApJ, 887, 93
Gvaramadze, V. V., Gualandris, A., & Portegies Zwart, S. 2009, MNRAS, 396, 570
Hayes, C. R., Majewski, S. R., Hasselquist, S., et al. 2020, ApJ, 889, 63
Heber, U., Edelmann, H., Napiwotzki, R., Altmann, M., & Scholz, R.-D. 2008, A&A, 483, L21
Hills, J. G. 1988, Natur, 331, 687
Hopkins, P. F. 2015, MNRAS, 450, 53
Huang, Y., Li, Q., Zhang, H., et al. 2021, ApJL, 907, L42
Ibata, R. A., Gilmore, G., & Irwin, M. J. 1995, MNRAS, 277, 781
Johnson, D. R. H., & Soderblom, D. R. 1987, AJ, 93, 864
Jurić, M., Ivezić, Ž, Brooks, A., et al. 2008, ApJ, 673, 864
Koposov, S. E., Boubert, D., Li, T. S., et al. 2020, MNRAS, 491, 2465
Laevens, B. P. M., Martin, N. F., Sesar, B., et al. 2014, ApJL, 786, L3
Li, H., Hammer, F., Babusiaux, C., et al. 2021, ApJ, 916, 8
Li, T. S., Koposov, S. E., Zucker, D. B., et al. 2019, MNRAS, 490, 3508
Lindegren, L., Bastian, U., Biermann, M., et al. 2021a, A&A, 649, A4
Lindegren, L., Klioner, S. A., Hernández, J., et al. 2021b, A&A, 649, A2
Liu, C., Fu, J., Shi, J., et al. 2020, arXiv:2005.07210
Luri, X., Brown, A. G. A., Sarro, L. M., et al. 2018, A&A, 616, A9
Majewski, S. R., Schiavon, R. P., Frinchaboy, P. M., et al. 2017, AJ, 154, 94
Marchetti, T. 2021, MNRAS, 503, 1374
McConnachie, A. W., & Venn, K. A. 2020a, RNAS, 4, 229
McConnachie, A. W., & Venn, K. A. 2020b, AJ, 160, 124
McMillan, P. J. 2017, MNRAS, 465, 76
Miyamoto, M., & Nagai, R. 1975, PASJ, 27, 533
Montanari, F., Barrado, D., & García-Bellido, J. 2019, MNRAS, 490, 5647
Navarro, J. F., Frenk, C. S., & White, S. D. M. 1997, ApJ, 490, 493
Portegies Zwart, S. F. 2000, ApJ, 544, 437
Poveda, A., Ruiz, J., & Allen, C. 1967, BOTT, 4, 86
Randich, S., Gilmore, G., Dd, D. & Gaia-ESO Consortium 2013, Msngr, 154, 47
Springel, V. 2005, MNRAS, 364, 1105
Steinmetz, M., Guiglion, G., McMillan, P. J., et al. 2020b, AJ, 160, 83
Steinmetz, M., Matijevič, G., Enke, H., et al. 2020a, AJ, 160, 82
Tauris, T. M. 2015, MNRAS, 448, L6
Tauris, T. M., & Takens, R. J. 1998, A&A, 330, 1047
Tsantaki, M., Pancino, E., Marrese, P., et al. 2022, A&A, 659, A95
Vasiliev, E., & Baumgardt, H. 2021, MNRAS, 505, 5978
Vasiliev, E., & Belokurov, V. 2020, MNRAS, 497, 4162
Vasiliev, E., Belokurov, V., & Erkal, D. 2021, MNRAS, 501, 2279
Wang, B., & Han, Z. 2009, A&A, 508, L27
Wang, B., Justham, S., & Han, Z. 2013, A&A, 559, A94
Yanny, B., Rockosi, C., Newberg, H. J., et al. 2009, AJ, 137, 4377
York, D. G., Adelman, J., Anderson, J. E., Jr., et al. 2000, AJ, 120, 1579
Yu, Q., & Tremaine, S. 2003, ApJ, 599, 1129
Zhao, G., Zhao, Y.-H., Chu, Y.-Q., Jing, Y.-P., & Deng, L.-C. 2012, RAA, 12, 723